Electrical conductivity of a strongly coupled plasma

George A. Rinker
Theoretical Division, Los Alamos National Laboratory, Los Alamos, New Mexico 87545
(Received 7 August 1984; revised manuscript received 5 November 1984)

This is the first in a series of papers concerning the electrical and thermal transport properties of dense plasmas. Temperatures and densities considered range approximately from room temperature to 10^4 eV and from 10^{-4} to 10^4 times compressed. In the present work we describe theoretical calculations of electrical conductivities using the t-matrix version of the Ziman theory with various self-consistent ionic potential models and realistic structure factors. The theoretical basis is described, and illustrative results are given.

I. INTRODUCTION

Since its inception over 20 years ago, the Ziman theory[1-8] has received much attention as a promising method for the calculation of electrical resistivities of disordered systems. The theory has been applied widely in numerical calculations of resistivities of liquid metals.[9-17] Substantial effort has been made to understand the formal properties of the theory, its limitations, and its potential for extension beyond its original range of physical validity.[18-30]

In the present work, we are interested in the electrical transport properties of plasmas. We have carried out an extensive set of numerical calculations based upon the Ziman theory. Our approach is pragmatic in that we view the models and parameters that appear as quantities that are to be specified in a physical way, both in the sense of agreeing with experimental data and in numerically approaching known asymptotic limits, and in satisfying requirements of internal theoretical consistency. This approach has led us to various model formulations of the Ziman theory. We have obtained results for a number of elements over temperatures ranging approximately from room temperature to 10^4 eV and densities ranging from 10^{-4} to 10^4 times normal. The principal improvement over previous work in this range of temperature and density is the elimination of errors due to the Born approximation, and the use of more realistic electron-ion potentials and ion-ion structure factors.

This paper is divided into four sections. In Sec. II we discuss the fundamental physical basis of the theory. Calculational and physical details are discussed in Sec. III, and selected numerical results are presented in Sec. IV. Further technical details of the calculation are collected elsewhere.[31,32] Future papers will deal with more extensive numerical results, comparisons with alternative approaches, and the closely related calculation of thermal transport coefficients.

II. BASIC PHYSICAL CONSIDERATIONS

The present work depends entirely upon a particular application of the so-called "average-atom" approximation: that the material of interest consists of a homogeneous medium into which is imbedded a static and statistically distributed collection of identical, nonoverlapping, and spherical scattering centers. The identical, nonoverlapping, and spherical assumptions are made in order to render the calculation tractable. By statistically distributed, we mean that the locations $\mathbf{r}_1$ and $\mathbf{r}_2$ of any two scattering centers are correlated by means of the usual two-body (ionic) correlation function $g_2(\mathbf{r}_1,\mathbf{r}_2)-1$, which enters into the theory through its Fourier transform $S(q)-1$. (Higher order correlations do not enter, for reasons which will quickly become apparent.) In principle, the homogeneous medium represents a region of constant potential between scattering centers through which electrons may propagate freely as plane waves. In practice, the homogeneous medium is a theoretical construct that contains a multitude of physical effects arising from the propagation of an electron through many scattering centers rather than through free space.

It is assumed that there is a certain density Z_i/Ω_0 of free electrons, described by a density matrix $\rho_e(t)$, free to propagate in the interstitial region. To calculate the resistivity, one applies an external electric field $\mathbf{E}$ and uses the linear response limit to express the perturbation in terms of the average retarding force on the electrons $\langle\mathbf{F}\rangle=\mathrm{Tr}[\rho_e(t)\mathbf{F}]$. This force is linearized in the electron current $\mathbf{J}$ and set equal to $-eZ_i\mathbf{E}$. Only the lowest nontrivial term in the multiple-scattering series for the electron propagator is considered (single-site scattering approximation). Classically, this may be viewed in the mean-free-path approximation: an electron is accelerated in the interstitial region by the external electric field until it collides with a scattering center, is accelerated and scattered again, and so on. The average distance traveled between scatterings, the magnitude and angular dependence of the scattering cross section, and the initial electron velocity all enter into a calculation of the resulting average electron current. In particular, the fact that the mean free path is finite puts an upper limit on the momentum that can be gained between scatterings, so that the conductivity is proportional to some increasing function of the mean free path. The mean free path depends upon the length scale set by the ionic separation distance. In the Ziman theory, the analog of this ionic separation is the two-body ionic correlation function $g_2(\mathbf{r}_1,\mathbf{r}_2)-1$, whose

Fourier transform $S(q)-1$ enters directly into the expression for the resistivity. The average electron velocity enters statistically through the Fermi-Dirac distribution function. The cross section $\sigma_\epsilon(q)$ and the density of free electrons Z_i/Ω_0 are to be computed from some suitable prescription appropriate for the material of interest.

Adopting the above physical assumptions and working through a rather lengthy derivation, Evans *et al.*[26] obtained what is known as the t-matrix formulation of the Ziman theory:

$$\eta=-\frac{1}{3\pi\alpha}\left[\frac{\Omega_0}{Z_i}\right]^2\frac{1}{\Omega_0}$$
$$\times\int_0^\infty d\epsilon\frac{d}{d\epsilon}f_{\beta\mu}(\epsilon)\int_0^{2p}dq\,q^3S(q)\sigma_\epsilon(q)\,, \tag{1}$$

where η is the resistivity, Z_i is the number of free electrons per atom (ionization state), Ω_0 is the atomic volume, $f_{\beta\mu}(\epsilon)$ is the Fermi-Dirac distribution function

$$f_{\beta\mu}(\epsilon)=(e^{\beta(\epsilon-\mu)}+1)^{-1}\,, \tag{2}$$

β ($\equiv 1/kT$) is the inverse temperature, μ is the chemical potential, $S(q)$ and $\sigma_\epsilon(q)$ are the ionic structure factor and the electron-ion cross section for momentum transfer $\mathbf{q}=\mathbf{p}'-\mathbf{p}$ and incident energy ϵ, and $\alpha\simeq 1/137.036\,04$. The momentum p is related to the energy ϵ by means of the usual relativistic dispersion relation

$$p^2=(E-V_z)^2-M^2$$
$$=(2M+\epsilon)\epsilon\,, \tag{3}$$

where M is the electron mass and V_z is the constant potential representing the homogeneous medium surrounding the ion sphere. In the above, we have written $E=\epsilon+M+V_z$, so that E is the total energy and ϵ is the kinetic energy. We refer to positive-energy states or continuum states with the understanding that we mean states with $\epsilon>0$ or $E>M+V_z$. Energy, momentum, and mass are measured in units of inverse length. Conventional units are resurrected by inserting the obvious factors of $\hbar$ and c, where $\hbar c\simeq 1.9732\,858\times 10^{-4}$ eV cm.

Equation (1) differs from the original Ziman formula in that the cross section $\sigma_\epsilon(q)$ replaces the Fourier transform of a weak pseudopotential; i.e., a partial-wave analysis replaces the Born approximation for $\sigma_\epsilon(q)$. Thus the t-matrix formulation removes this particular objection for systems that scatter electrons strongly, such as transition metals, where pseudopotential theory fails.

The mass M appearing in Eq. (3) is the mass of the free electron in the original Ziman (single-site scattering) approximation, which is valid in the weak-scattering limit, i.e., where the mean free path is large compared with the ionic radius. For more strongly interacting systems, however, one must question the validity of the single-site approximation.[33–38] One possible improvement is to attempt to generalize explicitly the Ziman theory to higher order terms in the multiple-scattering series. To our knowledge, this has not been done successfully. Another approach is to attempt to approximate the effects of higher order scattering by renormalizing[39] the electron mass (and possibly the external potential V_z). This roughly amounts to expressing the additional scattering effects by attributing a viscosity to the surrounding medium. There are various procedures by which one might attempt to calculate such an effective mass, but they all reduce to evaluating the multiple-scattering series in some approximation. Alternatively, one could simply take the effective electron mass and V_z as parameters to be fitted. None of these approaches is entirely satisfactory at present, however, so in the present work we simply take M to be the free-electron mass and leave this question open.

It should also be noted at this point that we use relativistic kinematics throughout our calculations. There is a certain inconsistency in this in that Eq. (1) was derived using explicit nonrelativistic forms for the wave functions and dispersion relation (3). We have not verified that a relativistic derivation would lead to Eq. (1). We have chosen relativistic kinematics, however, because (1) we are thereby able to retain a valid and consistent kinematical description of the electron motion at very high temperatures; (2) we are able to make direct contact with some existing relativistic atomic and ionic computer codes; and (3) the formulation is only slightly more complicated and the numerical effort only slightly greater. The only serious difficulty in such an approach is that the temptation exists to mix relativistic and nonrelativistic kinematics in an inconsistent way, which can lead to spurious and unphysical effects.[40] For the present calculations, we find that this subject is not quantitatively important. In no case considered so far have we found relativistic effects to alter the resistivity by more than a few percent.

To evaluate Eq. (1) for a given temperature and density, we need to specify (a) the free-electron density Z_i/Ω_0, (b) the chemical potential μ, (c) the electron-ion scattering cross section $\sigma_\epsilon(q)$ for energies within a few $kT=\beta^{-1}$ of the chemical potential, and (d) an appropriate ion-ion structure factors $S(q)$. There is no formal reason that these cannot be chosen independently of each other, as there is no rigorous requirement in the theory that they be internally consistent. In fact, the most notable quantitative successes of the Ziman theory have occurred for weak-scattering liquid metals at melting point, where experiments have allowed the construction of accurately parametrized pseudopotentials, structure factors, and ionization states.[41–50] Attempts have been made to provide a more formal basis for such calculations.[50–52] However, except for a rather limited temperature and density regime around melting point, accurate psuedopotentials are not available, and one must look for guidance to more theoretical approaches. Ideally, one would like to have an ionic model that yielded a reasonable density of states, electron-ion scattering cross section, and two-body ion-ion interaction so that one could calculate the electronic properties and the structure factor in an internally consistent way.[53] The best ionic models at present, however, depend upon the mean-field approximation, which fails in some important ways to reproduce known shell structure and which does not necessarily yield good ionic structure factors.

We have chosen to model the system in the following way (see Fig. 1). We construct a potential $V(r)$ for $r<r_t$,

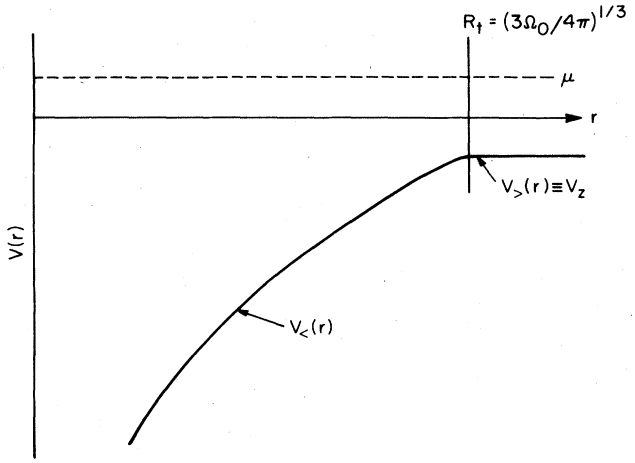

FIG. 1. Ionic model parameters.

the Wigner-Seitz radius

$$\Omega_0 = \tfrac{4}{3}\pi r_t^3 = \frac{A}{N_0 \rho} , \tag{4}$$

and adopt a prescription for the parameter V_z appearing in Eq. (3). In the above, A is the atomic mass, N_0 is Avogadro's number, and ρ is the material density in grams per unit volume. This is sufficient to determine the electronic density of states $dN_e/d\epsilon$ and cross section $\sigma_\epsilon(q)$ as a function of energy.[31,32] From the density of states, we determine the chemical potential μ so that the total amount of charge within the ion sphere is zero:

$$Z = \int_{-\infty}^{\infty} d\epsilon f_{\beta\mu}(\epsilon) \frac{dN_e}{d\epsilon} . \tag{5}$$

This is sufficient to insure overall neutrality of the system, although it is not the only procedure that could be adopted. The number of free electrons per atom is then computed from

$$Z_i = \int_0^{\infty} d\epsilon f_{\beta\mu}(\epsilon) \frac{dN_f}{d\epsilon} , \tag{6}$$

where the free-electron density of states is

$$\frac{dN_f}{d\epsilon} = \frac{\Omega_0}{\pi^2} p(M+\epsilon) . \tag{7}$$

This is not the same as the number of continuum electrons (those with $\epsilon > 0$):

$$Z_c = \int_0^{\infty} d\epsilon f_{\beta\mu}(\epsilon) \frac{dN_e}{d\epsilon}$$

$$= Z - \sum_{\substack{\text{bound} \\ \text{states}}} 2 |\kappa_b| f_{\beta\mu}(\epsilon_b) , \tag{8}$$

since the true density of states $dN_e/d\epsilon$ is not the same as the free-electron density of states $dN_f/d\epsilon$. This choice is made conventionally because if one sets V_z in Eq. (3) equal to the ionic potential at r_t, the electron density given by Eq. (6) is equal to the electron density at the boundary of the ion. Physically, the difference between the number of continuum and free electrons reflects the fact that in an attractive potential, some of the continuum electrons remain in the vicinity of the ion and are not actually free to participate in conduction.

The principal virtue of the above approach is that it leads to internally consistent calculations of the chemical potential, free-electron density, and scattering cross section. These quantities are all calculated using a full and highly adaptive partial-wave analysis, as described in detail elsewhere.[31,32]

III. MODEL DETAILS

A. Potentials

In principle, we can choose any local potential to represent the electron-ion interaction (explicitly nonlocal potentials are beyond the scope of the present approach). This potential need not be weak. It could be state dependent and energy dependent, but so far we have not investigated these complications seriously. We restrict consideration to potentials which are fundamentally theoretical and avoid extensively parametrized interactions on the grounds that *ad hoc* parametrizations are unlikely to be realistic very far from the regions in which the parameters are fitted.

For the isolated atom, the most successful theory at present which meets these criteria is based upon the self-consistent, relativistic Hartree-Fock-Slater mean-field approximation (MFA).[54] We require our ionic potentials to approach this in the low-density, low-temperature limit.

For high temperatures and densities, the corresponding limit is the temperature-dependent Thomas-Fermi-Dirac (TFD) approximation.[55] This method is also self-consistent, but the true solutions of the Dirac equation are replaced by plane waves for the appropriate r-dependent local momentum. The states themselves are populated according to the correct statistical weight Eq. (2), and the correct finite-volume boundary conditions at r_t are applied.

For intermediate regions of temperature and density, neither of these approximations is appropriate. A more sophisticated model has been developed by Liberman[56] in an attempt to incorporate the desirable features of both. This is essentially a TFD calculation with an improved (but still local) exchange approximation, with shell corrections obtained by exact solution of the Dirac equation for the important electronic states. Alternatively, one could call it an MFA calculation corrected for finite-volume boundary conditions and elevated-temperature statistical populations. This model effectively provides a physical interpolation between the MFA and TFD limits and will be referred to as AIJ (atom in jellium).

Two questions of fundamental importance concerning these potentials are the choice of a local approximation for the true nonlocal exchange interaction, and the choice of boundary condition as $r \to \infty$. These are related. The correct Hartree-Fock boundary condition for the neutral isolated atom is $V(r) \sim r^{-1}$ as $r \to \infty$. Any local exchange approximation proportional to some power of the density,

however, produces a potential which approaches a constant exponentially because of the requirement of charge neutrality and the fact that the wave-function tails decay exponentially. This boundary condition is important in the present context because it dictates the occupations of the valence states and the positions of the shape resonances.

Various schemes are used to overcome this difficulty while retaining locality and state independence. They collectively amount to attaching an inverse-r tail to the potential at some appropriate radius.[54,57,58] Figure 2 illustrates this process. The dot-dashed curve is the self-consistent potential obtained for Fe using Kohn-Sham exchange.[59–61] The dashed curve uses the same exchange approximation inside a certain radius r_1 but sets the potential to r^{-1} beyond r_1. Here r_1 is chosen as the radius which encloses $Z-1$ units of charge.[58] The discontinuity at r_1 arises from the exchange potential, as this prescription would make a pure electrostatic potential continuous by definition. The solid curve uses the same prescription but further modifies the interior potential by adding a constant to make it continuous at r_1. This effectively modifies the exchange so that it approaches zero at r_1 and produces a result intermediate between the previous two.

One can imagine further ways to accomplish similar results. There appears to be no completely satisfactory alternative, as the approaches discussed so far in the literature either give up the energy variational principle or produce unphysical results such as discontinuous potentials. This later difficulty is more important in the present context, as a potential discontinuity represents a rather peculiar charge distribution shell (proportional to a δ function and its derivative), which produces anomalous, unphysical, and sometimes large contributions to the scattering cross section. In contrast, we are not directly interested in total binding energies or entropy, so that a variational principle for the energy or free energy is not directly relevant. We therefore adopt the uniform physical requirement that potentials must be continuous everywhere.

This is sufficient to define the isolated atom (MFA) potential uniquely for a given electronic configuration, along with the r^{-1} boundary condition as $r\to\infty$, the above prescription for r_1, and specification of Kohn-Sham exchange otherwise for the interior potential. It furthermore defines the parameter V_z when we adapt the MFA potential to finite atomic volume by truncating it at r_t.

A similar question arises when we consider the TFD and AIJ models applied directly to nonzero temperatures and densities. The TFD potential is continuous at r_t by construction and probably exhibits the highest degree of internal consistency of those considered here. AIJ, however, does not share this virtue. As originally formulated, AIJ is based upon a variational principle for the free energy, from which the thermodynamic properties are obtained. This is optimum in the sense that these properties are then insensitive to first-order errors in the wave function. This does not imply, however, that other quantities (such as scattering amplitudes) obtained directly from the wave function and not the free energy will exhibit the same quality. One normally finds that the original version of AIJ produces a small discontinuity in the potential at r_t (see Fig. 3). This is evidently unphysical and reflects the constraints imposed by the approximate form assumed for the wave function, from which the free energy is calculated. It is not related to the discontinuity in the MFA potential. We find that the low-energy scattering amplitudes are rather sensitive to this discontinuity and that our results are improved in general if AIJ is constrained to produce a continuous potential. Such a modification is inconsistent with the original variational principle, however, and we expect that any thermodynamic properties so obtained would be less accurate than those from the original. It may be possible to reformulate AIJ with a different variational principle so that the free energy is minimized and the potential is naturally continuous, but we have not pursued this question here.

In general, we expect that the best results of the three are to be obtained from this model and have seen no serious numerical evidence to the contrary. However, we find that over much of our range of interest, this model produces results which are indistinguishable from TFD or MFA. For calculational simplicity, we have therefore adopted for most of our routine calculations a procedure which uses TFD potentials to provide the dependence upon temperature and density, combined with an MFA or

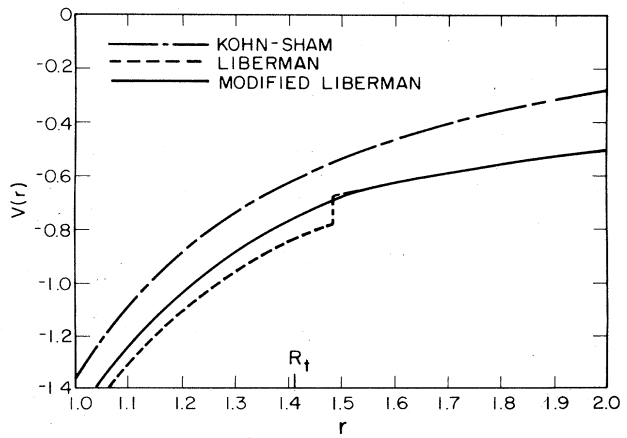

FIG. 2. Self-consistent atomic potential (MFA) for iron, with the configuration $3d^74s^1$.

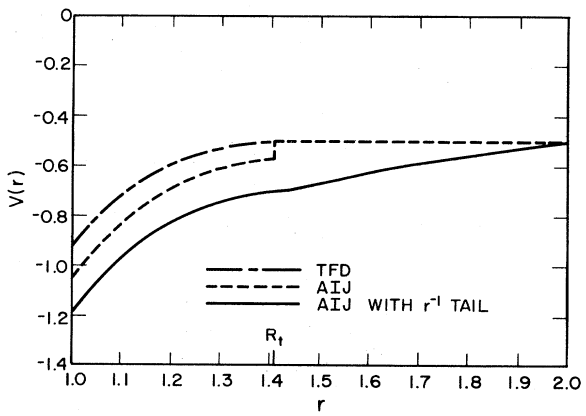

FIG. 3. Self-consistent finite-volume ionic potentials for iron, at $\rho=7.86$ g/cm^3 and $T=0.1$ eV.

AIJ potential chosen to establish the low-temperature, low-density limit. We adopt a numerical mixing formula

$$V(r)=\frac{V_0(r)+\xi V_T(r)}{1+\xi}\ , \tag{9}$$

where $V_0(r)$ is the appropriate low-temperature, low-density potential and $V_T(r)$ is the TFD potential computed for the temperature and density of interest. The mixing parameter ξ is given by

$$\xi=(T/T_0)^{\zeta_1}+(\rho/\rho_0)^{\zeta_2}\ , \tag{10}$$

where T_0 and ρ_0 are parameters of order 100 eV and 100 g/cm^3, and the exponents ζ_1 and ζ_2 are normally taken to be unity. These choices are made so that the mixing is done smoothly as a function of temperature and density and the correct limits are obtained. The results are not sensitive to these parameters.

The choice of $V_0(r)$ is made separately for each element based upon trial calculations, which are principally (but not exclusively) comparisons with measured melting-point resistivities. Our usual goal is to populate the known conduction-band electron states and come within a factor of 2 of the measured liquid resistivity, without sacrificing theoretical sensibility. We use no adjustable parameters in the AIJ calculations. For the MFA calculations, we are free within limits to adjust occupations of the valence states. We find occasionally that such adjustment is necessary in order to reproduce the conduction-band structure realistically.

In constructing the mixed potentials, a consistent set of boundary conditions must be chosen. The only procedure which is completely consistent with the criteria mentioned previously is to set $V_0(r_t)=V_T(r_T)=V_z$. This can be done by adding a constant to $V_0(r)$, which obviously does not alter any physical results obtained from it. This process is well defined for the atomic potential, truncated, and made continuous. If we have chosen a melting-point AIJ potential for $V_0(r)$, however, we must extrapolate it beyond r_t (melt) if we are to use it for lower densities. As long as we retain the continuity requirement and r^{-1} boundary condition as $\rho\to 0$, our choices reduce to adopting a scheme for attaching an inverse-r tail. A simple procedure which we have used in some calculations is to attach this tail at r_t (melt). This seems to work reasonably well, but we regard this matter to be open to experimentation and improvement.

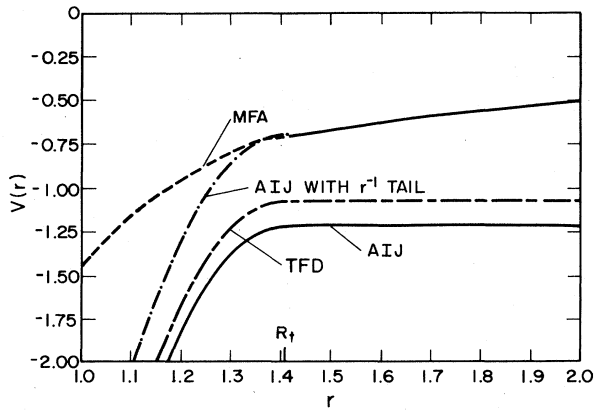

FIG. 4. Self-consistent potentials for iron, at $\rho=7.86$ g/cm^3 and $T=10^3$ eV. The mixed potential used in the tabulated calculations is approximately 0.9 times the TFD potential shown plus 0.1 times the AIJ potential (solid line) shown in Fig. 3.

Figure 4 shows some of these potentials for Fe at $\rho=7.86$ g/cm^3 and $T=10^3$ eV. The MFA (dashed curve) is quite different from the others. The TFD and AIJ potentials are virtually identical except for an additive constant. The AIJ discontinuity at r_t has nearly vanished because of the importance of relatively energetic electron states. The dot-dashed curve illustrates the procedure of attaching an inverse-r tail to the AIJ potential.

B. Structure factors

We have used various models for the structure factor, which in our approach does not have an explicit connection to the electron-ion potentials. At melting point, it is well known that the Percus-Yevick structure factor can accurately be fit to neutron-diffraction data.[62–66] For high temperatures, however, this structure factor is inappropriate. We have also carried out calculations using the Debye-Hückel structure factor

$$S(q)=\frac{q^2r_d^2}{(1+q^2r_d^2)}\ , \tag{11}$$

where

$$r_d^2=\frac{r_t^2}{3\Gamma} \tag{12}$$

is the Debye radius, with the ion-ion coupling constant Γ, given by

$$\Gamma=\frac{Z_i^2\alpha\beta}{r_t}\ . \tag{13}$$

A third choice is based on the correlation function

$$\begin{aligned} g(r)&=0, \quad r<r_c \\ &=\frac{B}{r}e^{-r/r_d}+1, \quad r\geq r_c \end{aligned} \tag{14}$$

where r_c is a core exclusion radius, taken as an adjustable parameter, and B is the normalization constant required to conserve probability. This yields the structure factor

$$\begin{aligned} S(q)=1&-\frac{3}{(qr_t)^3}[\sin(qr_c)-qr_c\cos(qr_c)] \\ &-\frac{1-(r_c/r_t)^3}{qr_d(1+r_c/r_d)}\frac{\sin(qr_c)+qr_d\cos(qr_c)}{1+(qr_d)^2}\ . \end{aligned} \tag{15}$$

This third structure factor Eq. (15) has the virtue that it approaches the Debye-Hückel limit Eq. (11) as $r_c\to 0$, and the simple hard-sphere limit

$$S(q)=1-\frac{3}{(qr_t)^3}[\sin(qr_c)-qr_c\cos(qr_c)]\ , \tag{16}$$

based on the correlation function

$$g(r)=0, \quad r<r_c$$
$$=1, \quad r\geq r_c \tag{17}$$

as $r_d\rightarrow\infty$. This third structure factor is close to the Percus-Yevick solution on the average, although the secondary structure is different. It is similar to what is known in the literature as the mean spherical approximation.[67,68] We have also made calculations using one-component plasma structure factors.[69,70] We find little difference in general, although some elements show sensitivity near melting point.

Figure 5 compares the structure factors for Fe at melting point. We have also chosen a core exclusion radius corresponding to a packing fraction 0.45 at $T=0$ for both the Percus-Yevick and third structure factors. This value is known to give good results in general for Percus-Yevick structure factors for liquid metals at melting point. We adopt it for the third structure factor in order to retain reasonable connection with Percus-Yevick at these tempertures and densities. As noted above, the third structure factor approximates Percus-Yevick on the average but does not reproduce the oscillations.

Figure 6 compares these three structure factors at $T=1$ eV and $\rho=\rho_0/8192\simeq 9.59\times 10^{-4}$ g/cm^3. The transition to the Debye-Hückel form is evident. We have introduced a temperature dependence into the core exclusion radius for the third structure factor in the following way. We assume that at high temperature, the repulsive interaction energy $Z_i^2\alpha/2r_c$ between two ions at closest approach is proportional to the temperature. At low temperature, we wish to retain the $T=0$ hard-sphere limit corresponding to a packing fraction 0.45. The form

$$\frac{r_t}{r_c}=\frac{1}{0.766}+\frac{2C}{\Gamma} \tag{18}$$

serves this purpose, where $0.766^3\simeq 0.45$ is the $T=0$ packing fraction, Γ is the ion-ion coupling constant given above, and C is a dimensionless parameter of order unity. Some numerical experimentation suggests a value $C\simeq 2$,

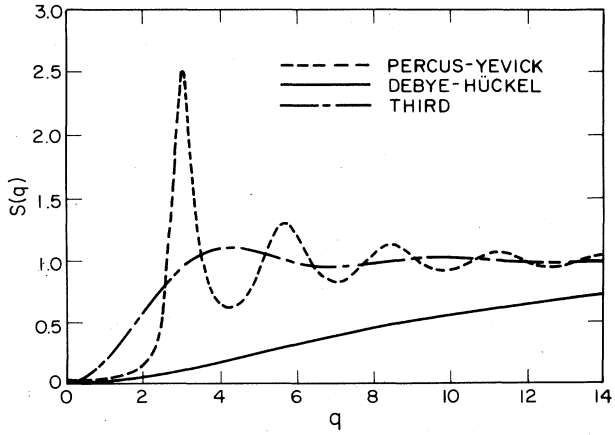

FIG. 5. Structure factors for iron at $\rho=7.05$ g/cm^3 and $T=0.156$ eV, with ionic charge $Z_i=0.936$ and packing fraction 0.45.

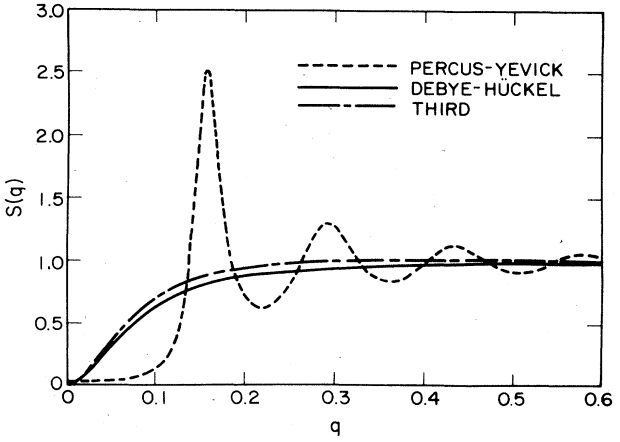

FIG. 6. Structure factors for iron at $\rho=9.59\times 10^{-4}$ g/cm^3 and $T=1$ eV, with ionic charge $Z_i=1.73$ and packing fraction 0.45.

which we have used in most calculations so far. Calculated resistivities are fairly insensitive to this choice.

C. Calculational procedures

The most serious technical problem concerns the calculation of the density of states $dN_e/d\epsilon$ and the cross section $\sigma_\epsilon(q)$ to the point of convergence in κ and on an energy grid sufficient to carry out the integrals in Eqs. (1) and (5) accurately enough. Most of the structure in these sums and integrals comes from the bound states and shape resonances that an ion will exhibit in general at a given temperature and density. The behavior of some of these states near threshold is indicated in Fig. 7, where we have plotted the kinetic energy ϵ of each high-lying state as a function of density for $T=0$. When an s state enters the continuum, it becomes a resonance which remains at zero energy and quickly spreads out over all momenta, thus disappearing as a recognizable entity and eventually contributing a small increase to the free-electron-like

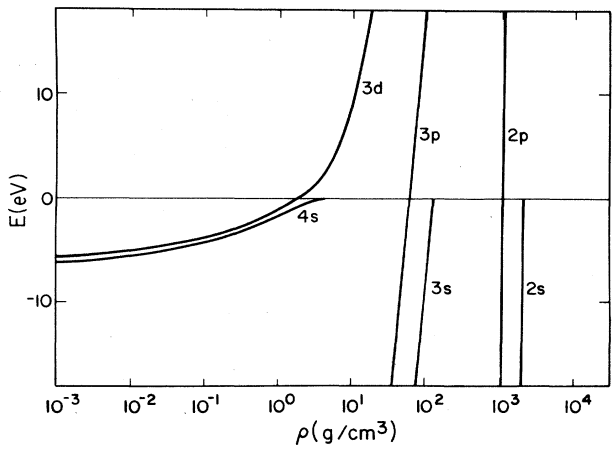

FIG. 7. Level energies of various electron states in iron as a function of density.

background. For $l\neq 0$, however, ionization of a bound state invariably produces a shape resonance, which can then be followed high into the continuum as it broadens and eventually disappears.

These two kinds of states thus affect the conductivity differently as they are ionized. Ionization of an s state produces a more dramatic change in the chemical potential and thus a sometimes large change in the energies at which the scattering cross section is evaluated. This may produce an increase or a decrease in the conductivity, depending upon whether the chemical potential is moved into or away from a resonance that already exists in the calculation. Ionization of an $l\neq 0$ state, however, normally produces no such dramatic effect, as the charge in the bound state remains localized as it is carried into the continuum, contributing more to conduction as it gradually spreads out. Physically, the shape resonances represent nearly bound states which contribute strongly to the scattering. They contribute to the calculation of the chemical potential in that they represent electrons which remain largely in the vicinity of the ion, containing a relatively large amount of charge without being free to contribute significantly to conduction.

Figure 8 shows a calculated density of states for iron at melting point. Also plotted is the Fermi-statistical weighting factor Eq. (2). These resonances (d wave) account for most of the charge in the continuum. For iron at this density, approximately 18 electrons go into bound states. The sharp d-wave resonances can accommodate nearly 10 electrons, thereby guaranteeing that the 8 remaining electrons will go mostly into these resonances and produce a chemical potential which lies within the resonance. This corresponds to the well-known fact that the conduction electrons lie in the d band and scatter strongly even in the liquid phase.[71] The number of free electrons as calculated from Eq. (6) is much smaller, as expected. This quantity depends somewhat upon the potential model used, as a model which shifts the resonance energy (and thus the chemical potential) directly affects the number of free electrons through Eq. (6).

In Fig. 9 we have plotted phase shifts as a function of the external momentum p for the first six spin-up states. Phase shifts for the spin-down states are virtually identical for these energies. We have chosen the convention

$$\delta_\kappa(0)=n_\kappa\pi\ , \tag{19}$$

where n_κ is the number of bound states for angular momentum κ. Our phase shifts thus satisfy Levinson's theorem with $\delta_\kappa(\infty)=0$, $\delta_\kappa(\epsilon)>0$ for all $\epsilon>0$. The figure shows clearly the d-wave phase shift increasing rapidly through $\pi/2$ at the resonance energy. Figure 10 shows the resistivity integrand

$$\Sigma(\epsilon)=\int_0^{2p} dq\, q^3 S(q)\sigma_\epsilon(q) \tag{20}$$

along with the Fermi-factor derivative

$$f'_{\beta\mu}(\epsilon)=-\beta f_{\beta\mu}(\epsilon)[1-f_{\beta\mu}(\epsilon)] \tag{21}$$

over which $\Sigma(\epsilon)$ is to be integrated.

The sharpness of such resonances causes an inherent problem of physical significance. In the first place, any average-atom, single-particle model exaggerates what is otherwise a natural resonance structure. There are several effects which are not incorporated here which serve to broaden such resonances. In the liquid, local fluctuations in temperature, density, deformation, and ionization state will all serve to produce broader effective resonances when averaged over some statistical ensemble than are calculated for one particular "average" ion.[72–75] The existence of such effects is clearly demonstrated by the sharp change (a factor of the order of 2) which is experimentally observed in the resistivity upon melting. In addition, the momentum p of an incoming electron is indeterminate by means of the uncertainty principle to within $\sim\lambda^{-1}$, where λ is the electron mean free path. We should emphasize that any approach based formally upon the Ziman theory suffers from these limitations, since one ultimately evaluates cross sections and densities of states for a single ion which is taken in some sense to be

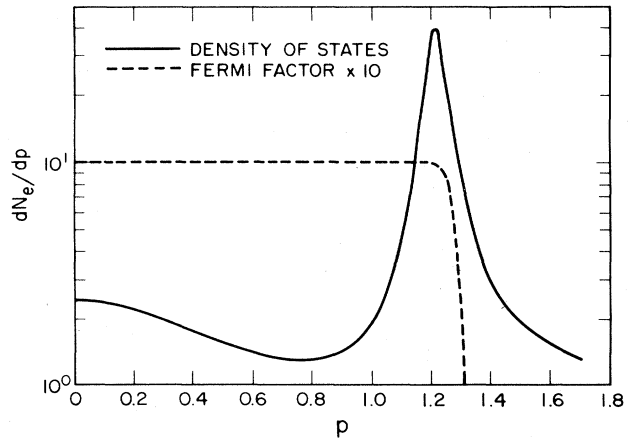

FIG. 8. Density of states and $f_{\beta\mu}(\epsilon)$ (plotted as functions of the momentum p) for iron at $\rho=7.05$ g/cm^3 and $T=0.156$ eV. Plotted is the ratio of the calculated to the free-electron density of states.

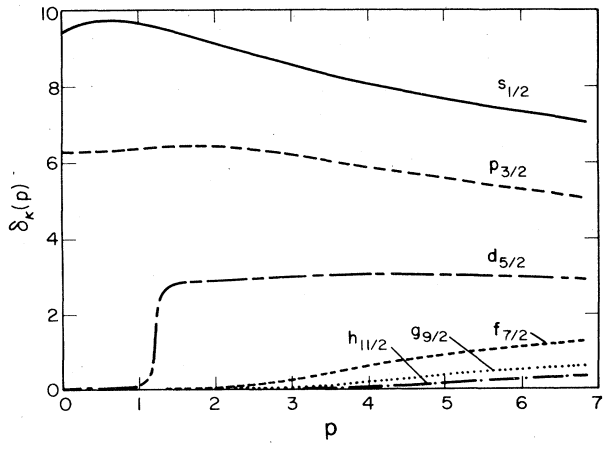

FIG. 9. Phase shifts for iron at $\rho=7.05$ g/cm^3 and $T=0.156$ eV.

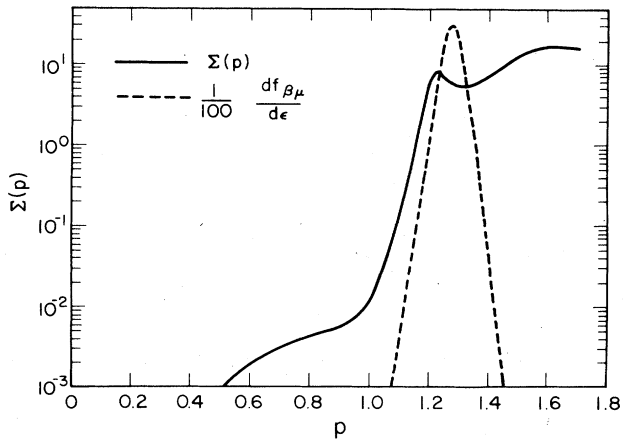

FIG. 10. The functions $\Sigma(\epsilon)$ and $df_{\beta\mu}(\epsilon)/d\epsilon$ (plotted as functions of the momentum p) for iron at $\rho=7.05$ g/cm^3 and $T=0.156$ eV.

representative of a statistical ensemble of ions. One should instead compute the electron current separately for a number of different ionic configurations and then take an appropriate ensemble average. The reason that these two approaches can yield different results is that the various quantities (ionization state, chemical potential, cross section) are highly nonlinear and erratic functions of the variables over which one should average.

We furthermore recognize that any spherically symmetric, uncorrelated single-particle ionic model produces an oversimplified and only approximately correct electronic level structure. It is well known, for example, that the $3d$ single-particle states of the isolated iron atom are fragmented into many levels distributed over a range in energy of several electron volts. This fragmenting may be attributed to the explicit electron-electron interaction which is neglected in the mean-field approximation. Unfortunately, it is currently not feasible to use more sophisticated theoretical models to produce more realistic level structure. Nor is it possible to incorporate detailed experimental level information in a systematic way, as this information is not available throughout most of the range of temperature and density of interest. It is therefore necessary to consider more approximate ways to make the resonance structure of our model more realistic.

Table I illustrates the sensitivity of our calculations to the position of the d-state resonances. Several different self-consistent potentials are used, and although the chemical potential falls within a few half-widths of the $d_{5/2}$ resonance in every case, the calculated resistivity varies by more than a factor of 10.

To ease these difficulties, we have adopted an artificial procedure to broaden the resonance structure. We are interested in the integrals

$$I_1=\int_0^\infty d\epsilon f_{\beta\mu}(\epsilon)\frac{dN_e(\epsilon)}{d\epsilon} \tag{22}$$

and

$$I_2=-\int_0^\infty d\epsilon f'_{\beta\mu}(\epsilon)\Sigma(\epsilon)\ . \tag{23}$$

We write the convolution

$$\frac{dN_e(\epsilon)}{d\epsilon}\rightarrow\int_0^\infty d\epsilon' h_w(\epsilon-\epsilon')\frac{dN_e(\epsilon')}{d\epsilon'} \tag{24}$$

and

$$\Sigma(\epsilon)\rightarrow\int_0^\infty d\epsilon' h_w(\epsilon-\epsilon')\Sigma(\epsilon')\ . \tag{25}$$

In these expressions, $h_w(\epsilon-\epsilon')$ is some suitable form factor of characteristic width w^{-1}, taken as a parameter to represent a physical width which we expect the resonances to have beyond what is predicted by our single-particle model. The above prescription effectively broadens structures in $dN_e/d\epsilon$ or $\Sigma(\epsilon)$ which have widths narrower than w^{-1} so that they have widths of order w^{-1} and does not significantly affect structures which are already broader than this.

If we let the lower limits in Eqs. (22)—(25) go to $-\infty$, with the understanding that $dN_e/d\epsilon$ becomes a sum of suitably weighted δ functions at the bound state energies for $\epsilon<0$, it is easy to show[31,32] that the result may be approximated by modification of the temperature β^{-1}. Such a procedure is simple to implement and has been used to calculate the resistivities in the last column in

TABLE I. Sensitivity to potential models. Energies are given in eV, resistivities η in $\mu\Omega$ cm.

Model	$E(d_{5/2})$	$\frac{1}{2}\Gamma(d_{5/2})$	μ	η	η (broadened)
AIJ No. 0	7.41	0.57	8.02	877	157
AIJ No. 1	8.43	0.68	9.07	1081	167
MFA No. 0	5.66	0.37	6.18	350	143
MFA No. 1	4.29	0.20	4.68	176	125
MFA No. 2	2.36	0.046	2.61	78	104
MIX[a]	5.71	0.39	6.25	365	147
TFD	27.06	7.21	22.03	130	119

AIJ No. 0: discontinuous at r_t
AIJ No. 1: continuous at r_t
MFA No. 0: electron configuration $3d^8 4s^0$
MFA No. 1: electron configuration $3d^7 4s^1$
MFA No. 2: electron configuration $3d^6 4s^2$

[a]MIX: mixed potentials.

Table I, using a convolution width of 4 eV with an exponential form factor. The width, 4 eV, was chosen as representative of the observed fragmenting of the $3d$ states in the isolated iron atom. The effectively higher temperature makes the exact location of the chemical potential with respect to the d-resonance energy much less important.

A problem arises with this temperature modification at very low temperatures and densities. Modifying the temperature effectively broadens the bound states as well as the continuum states, and if the folding width is comparable with the ionization potential of the isolated atom, the ionization state does not approach zero in this limit. It is then necessary to consider whether this broadening of the bound states represents a desirable physical modification, or if not, to use an explicit folding procedure to restrict broadening to the positive-energy functions only.

In the present work we have also carried out extensive calculations using this restricted broadening with explicit numerical folding procedures. As a practical matter, we use a form factor of exponential or Lorentzian shape in the momentum p rather than the energy ϵ, since we have chosen[31,32] p as our variable of integration in Eqs. (1), (5), and (6). We normally take a folding with w^{-1} of order $\Delta p \sim \lambda^{-1}$, but this choice is to some extent moderated by other considerations, the most important being whether the results so obtained are physically realistic.

To further illustrate this procedure and the nature of the average-atom approximation, we consider local density fluctuations in the liquid. Geometrical considerations preclude the possibility of packing a material of density ρ with spheres of radius r_t. Thus, if one restricts consideration to spherical ions, one should consider instead some ensemble of ions of different radii whose average radius in some suitable sense is r_t. To estimate what order of magnitude this variation in radius should have, we consider a cube of volume Ω_0. The inscribed sphere has volume $\simeq\Omega_0/2$, whereas the enclosing sphere has volume $\simeq 2.7\Omega_0$. Figure 11 shows resistivities calculated for Fe using several different applications of AIJ at

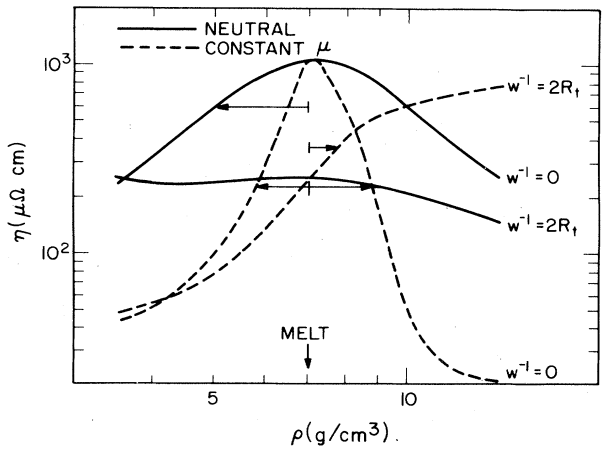

FIG. 11. Effect of density fluctuations. Resistivities calculated for iron at densities ranging from 3.525 g/cm^3 to 14.1 g/cm^3.

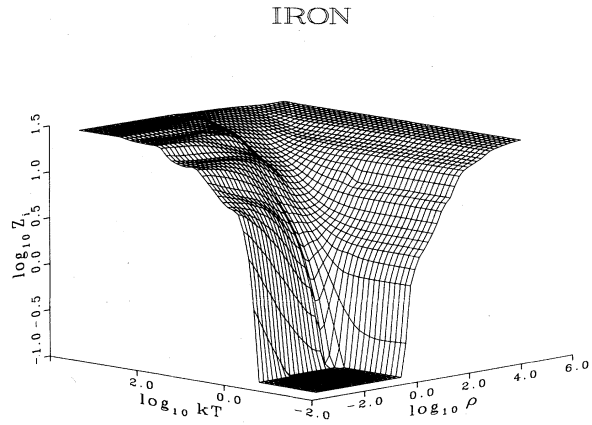

FIG. 12. Ionization state Z_i for iron for temperatures ranging from 0.031 25 eV to 8192 eV and densities ranging from 9.59×10^{-4} g/cm^3 to 6.44×10^4 g/cm^3.

$T=T$(melt)$=0.156$ eV, with the atomic volume allowed to vary over this approximate range. The solid curves are calculated allowing the chemical potential to vary with density as usual, so that the constraint Eq. (5) is satisfied at each point. The dashed curves fix the chemical potential at the ρ(melt)$=7.05$ g/cm^3 value, so that the ion spheres are neutral only in some overall average sense. We have carried out two sets of calculations for each case: one uses an exponential form factor and the broadening width $w^{-1}=2r_t$ in momentum space, and the other uses no broadening ($w^{-1}=0$). Simple numerical averages are also shown as horizontal lines connected to the corresponding curves. In only one case is the mean value close to the value of the mean. For the calculations in which μ is fixed, the average electronic charge within the ion sphere is 24.7 for $w^{-1}=0$ and 25.9 for $w^{-1}-2r_t$. None of these averages can be taken to have a great deal of quantitative meaning, since we have not constructed a thermodynamically consistent statistical ensemble or averaging procedure. However, we can draw three con-

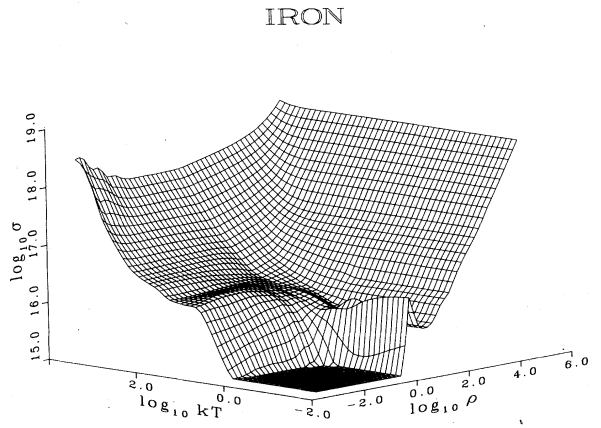

FIG. 13. Electrical conductivity σ (s^{-1}) for iron for temperatures ranging from 0.031 25 eV to 8192 eV and densities from 9.59×10^{-4} g/cm^3 to 6.44×10^4 g/cm^3.

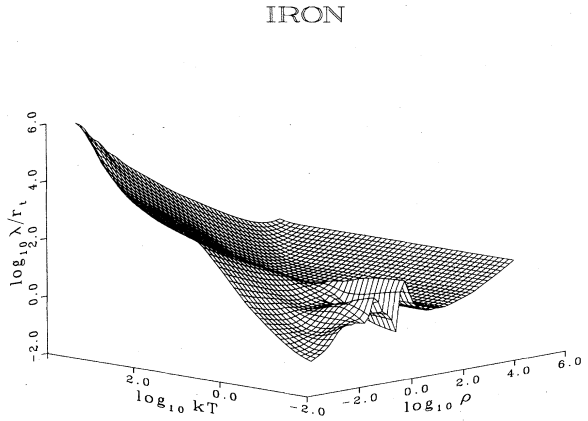

FIG. 14. Mean free path λ/r_t for iron for temperatures ranging from 0.031 25 eV to 8192 eV and densities ranging from 9.59×10^{-4} g/cm^3 to 6.44×10^{4} g/cm^3.

clusions from Fig. 11: (1) local fluctuations can produce erratic and unpredictable variations in the calculated resistivity; (2) the average-atom approximation can itself produce large errors in the calculated resistivity; and (3) as before, introduction of a resonance-broadening procedure can damp the effects of these fluctuations. As a warning, one should perhaps extract from Fig. 11 a nominal factor-of-2 uncertainty in the resistivity at any given temperature and density arising from the average-atom approximation. On an overall basis, however, this is too conservative. In a table of resistivities calculated over a range of temperature and density, we expect these fluctuations to produce structure in the curves without so seriously affecting their average values.

A further calculational difficulty arises in carrying out the partial-wave sums over angular momentum κ. For densities comparable with or greater than normal, the ionic radius is sufficiently small that it is feasible to carry out the complete partial-wave analysis. For densities less than normal, however, such a procedure becomes increasingly cumbersome because of the high number of partial waves required, even when the Born and Fermi gas approximations are used to accelerate convergence of the sums over angular momentum.[31,32] Although the calculation requires only a few partial waves at low incident electron energies, for high temperatures and low densities one must consider the scattering of high-energy electrons of large angular momentum. The maximum limit we have chosen is $|\kappa| \leq 96$, and even this large value is inadequate at temperatures of 8 keV and compressions of the order 10^{-2}.

We emphasize that the difficulty in accelerating convergence lies with the Born approximation and not the Fermi gas approximation for the density of states. This is because the Born approximation depends upon zeroth-order wave functions that are free plane waves, whereas the Fermi gas approximation uses plane waves that are better in the sense that they have been modified to yield the correct local momentum.

We have thus adopted semitheoretical methods to extrapolate our partial-wave results to low densities. These methods use various combinations of the partial-wave analysis along with the Born and Fermi gas approximations. The approximate nature of these calculations requires that adjustments be made in the potential, chemical potential, and cross section in order to insure continuity with the full partial-wave calculations, and to obtain the correct asymptotic limits as $\rho\rightarrow0$. These combinations and adjustments have so far been handled on a case-by-case basis and will be specified when individual calculations are discussed.

TABLE II. Comparison with Hubbard and Lampe. Resistivities η are given in $\mu\Omega$ cm.

	$Z=26$ $T=5$ keV $r_t=0.224\,19$ A		$A=55.85$ $\rho=7.86\times250=1965$ g/cm^3 $\Gamma=6.99$	
Model	Z_i	η	η previous model	% change
1	22.99	0.827		
2	22.99	0.649	0.78	−22
3	22.86	0.629	0.97	−3
4	23.33	0.640	1.02	+2
5	23.33	0.635	0.99	−1
6	23.33	0.399	0.63	−37
7	23.33	0.387	0.97	−3

1: TFD potential, combined structure factor
2: Same as 1 but Debye-Hückel structure factor
3: Same as 2 but screened Coulomb potential $r_s=0.48r_t=0.108$ A
4: Same as 3 but Born approximation
5: Same as 4 but nonrelativistic kinematics
6: Same as 5 but r_s=Lampe's value =0.048 A
7: Hubbard-Lampe calculation
Net difference = 7/1=0.47=−53%

IV. ILLUSTRATIVE RESULTS FOR Fe

In this section we display some results for Fe using the methods so far described. Figure 12 shows the ionization state Z_i for the range $0.031\,25\ \text{eV} \leq T \leq 8192\ \text{eV}$ and $\rho_0/8192 \leq \rho \leq 8192\rho_0$, with $\rho_0 = 7.86\ \text{g/cm}^3$. Figure 13 shows the corresponding conductivity $\sigma = 1/\eta$, in inverse seconds. The transition to insulator at $\rho \simeq 1.5\ \text{g/cm}^3$ is clearly evident in the figures. The local maxima at low T in Fig. 13 at $\rho \simeq 1.5\ \text{g/cm}^3$ is clearly evident in the figures. The local maxima at low T in Fig. 13 at $\rho \simeq 4\ \text{g/cm}^3$ are due to the ionization of the $3d$ and $4s$ levels, and the similar but less dramatic structure at higher density is due to the successive ionization of the $3p$, $3s$, $2p$, and $2s$ levels.

The value in Fig. 13 corresponding to $\rho(\text{melt}) = 7.05\ \text{g/cm}^3$ and $T(\text{melt}) = 0.156$ eV gives $\eta(\text{melt}) = c^2 \times 10^{-3}/\sigma(\text{melt}) = 117.8\ \mu\Omega\,\text{cm}$, to be compared with the experimental value $138.6\ \mu\Omega\,\text{cm}$. This level of agreement is somewhat better than we have a right to expect (note that no parameters were fitted). In general, we find at melting point that we obtain differences from experiment which vary up to a factor of 2 for no obvious reason. Differences larger than this can usually be attributed to a qualitatively incorrect description of the conduction band, implying that the melting-point potential used is wrong.

Figure 14 shows a classical mean free path:

$$\lambda = \frac{\sigma\Omega_0}{Z_i\alpha}\langle p^2\rangle^{1/2}\,, \tag{26}$$

which may be interpreted from these conductivities. To estimate an average momentum, we write

$$\langle p^2\rangle \int_0^\infty dp \frac{dN_f}{dp} f'(\epsilon) = \int_0^\infty dp \frac{dN_f}{dp} p^2 f'(\epsilon)\,. \tag{27}$$

This average selects those momenta near the Fermi momentum for the degenerate case, and approaches the ideal gas limit for large kT. Plotted is the ratio λ/r_t, which is greater than 1 for the most part. We take $\lambda/r_t \simeq 2$ to represent the metal-insulator transition at low temperature and density.

In the regions where comparisons may be made, the conductivities in Fig. 13 agree in general to within an approximate factor of 2 with those calculated by Lampe and Hubbard.[76–79] Other calculations appear in the literature.[80–92] The differences are larger (as much as an order of magnitude) at very low densities. This is apparently due to the error in the Born and Fermi gas approximations, discussed in Sec. III. The calculations displayed use the full partial-wave analysis for $\rho \geq 7.86\ \text{g/cm}^3$. For lower densities, only those bound states with $|\kappa| \leq 7$ and continuum states with $|\kappa| = 1$ are included exactly. Remaining states are treated in the Born and Fermi gas approximations. This necessitates adding an empirical correction to the approximate chemical potential to make it continuous across the boundary $\rho = 7.86\ \text{g/cm}^3$. This correction is necessarily a function of temperature. We have chosen to make it independent of density. Similarly, the resistivities are corrected by an overall empirical multiplicative factor depending upon temperature but independent of density. Some improvement could apparently be made by making this renormalization proportional to $(\rho/\rho_0)^{1/3}$, which is what one would expect if the error in the Born approximation is proportional to the maximum allowed classical angular momentum $l_{\max} = pr_t$. This trend in increasing error is suggested by the fact that for high temperatures, the curves in Fig. 13 rise toward lower density.

Table II shows a detailed comparison we have made with calculations using the method of Hubbard and Lampe for Fe at $T = 5\times10^3$ eV and $\rho = 250\rho_0 = 1965\ \text{g/cm}^3$. The initial difference between our results and theirs is a factor 0.47 (their resistivity is smaller than ours by 53%). We have decomposed this discrepancy by considering separately the differences in assumptions made in the two calculations. The difference in structure factor (reflected in their ionic screening function) amounts to a factor of 0.78. Using an exponentially screened Coulomb potential with screening radius r_s adjusted to approximate our TFD potential gives an additional factor 0.97. Using the Born approximation rather than a partial-wave analysis gives a factor of 1.02. Nonrelativistic kinematics gives a factor of 0.99. Using Lampe's potential screening parameter r_s rather than our fitted one gives a factor of 0.63. Finally, the ratio of our result to theirs using the above assumptions of theirs gives a net unexplained discrepancy of 0.97. This 3% difference between a Ziman calculation otherwise using their model and their result is evidently due to the difference in the fundamental transport equations that are solved, or simply to numerics. We do not consider it significant. The important differences are due to the structure factor and to the potential model used.

Figures 15 compares the present results with the electrical conductivity calculations of Hubbard and Lampe, as a function of temperature and density. Plotted is the ratio of our result to theirs, assuming in both cases the ionization states displayed in Fig. 14. In the regions of temperature and density where this ratio is set to 10^{-2}, Hubbard and Lampe do not consider their calculation to be valid. The ratio varies between $\frac{1}{2}$ and 2 throughout most of the

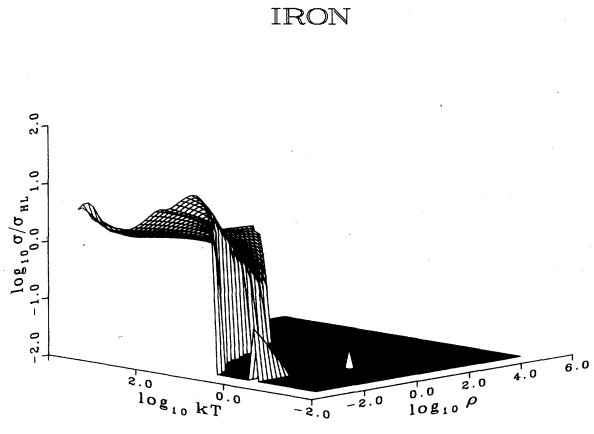

FIG. 15. Ratio of calculated electrical conductivity σ to that of Hubbard and Lampe σ_{HL}.

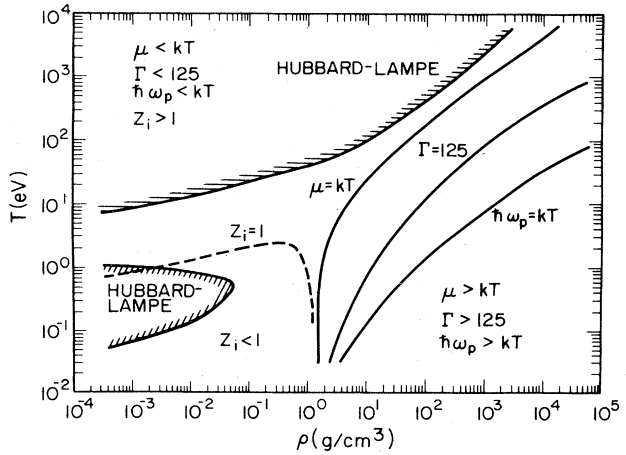

FIG. 16. Physical regions in the temperature-density plane.

region of high temperature and low density. The fact that it is not uniformly 1 apparently arises from errors in the Born approximation and differences in the structure factor.

Figure 16 shows the regions in the T-ρ plane bounded by the values $Z_i=1$, $\mu=kT$, $\Gamma=125$, and $kT=\hbar\omega_p$. Where Γ is large (i.e., $\Gamma\geq 125$) or $\hbar\omega_p \geq kT$, one can expect collective effects (plasma oscillations, crystallization) to interfere both through electron-phonon scattering and through coherence effects arising from the periodic structure of the material.[93,94] These effects are explicitly ignored here through our assumption of a disordered system. Additionally, the region $Z_i<1$ is suspect because of the extreme sensitivity of the results to details of the model potential. Throughout most of this latter region, however, the ionization state and conductivity are so low that they may be considered not significantly different from zero. Also shown in Fig. 16 are the regions in which Hubbard and Lampe consider their calculation to be valid.

ACKNOWLEDGMENTS

Much of the work reported here was developed from ideas arising in discussions with B. I. Bennett and D. A. Liberman. I would like to thank both of them for this stimulation and for the generous use of their computer codes. I would also like to thank A. L. Merts for the many useful hours of discussions of electrical and thermal transport, J. Abdallah for much assistance with library and graphics routines, and D. B. Boercker, C. W. Cranfill, R. B. Laughlin, Y. T. Lee, I. R. Lindemuth, R. M. More, and G. H. Nickel for their continued interest, useful ideas, and critical evaluation of this work. This manuscript was produced with the text editor-formatter TEDI, written by C. W. Nielson.

[1]J. M. Ziman, Philos. Mag. **6**, 1013 (1961).
[2]C. C. Bradley, T. E. Faber, E. G. Wilson, and J. M. Ziman, Philos. Mag. **7**, 865 (1962).
[3]J. M. Ziman, Adv. Phys. **13**, 89 (1964).
[4]J. M. Ziman, Proc. Phys. Soc. **86**, 337 (1965).
[5]J. M. Ziman, *Principles of the Theory of Solids* (Cambridge University, Cambridge, 1965).
[6]T. E. Faber and J. M. Ziman, Philos. Mag. **11**, 153 (1965).
[7]J. M. Ziman, Proc. Phys. Soc. **88**, 387 (1966).
[8]T. E. Faber, in *The Properties of Liquid Metals,* edited by S. Takeuchi (Wiley, New York, 1973).
[9]N. W. Ashcroft and J. Lekner, Phys. Rev. **145**, 83 (1966).
[10]O. Dreirach, J. Phys. F **1**, L40 (1971).
[11]R. Evans, Phys. Chem. Liq. **2**, 249 (1971).
[12]O. Dreirach, R. Evans, H.-J. Güntherodt, and H.-U. Künzi, J. Phys. F **2**, 709 (1972).
[13]G. Busch and H.-J. Güntherodt, in *The Properties of Liquid Metals,* edited by S. Takeuchi (Wiley, New York, 1973).
[14]A. Paskin, R. J. Harrison, and P. Ascarelli, in *The Properties of Liquid Metals,* edited by S. Takeuchi (Wiley, New York, 1973).
[15]V. K. Ratti and A. Jain, J. Phys. F **3**, L69 (1973).
[16]G. Busch and H.-J. Güntherodt, in *Electronic Properties of Liquid Methods and Alloys,* Vol. 29 of *Solid State Physics: Advances in Research and Applications,* edited by H. Ehrenreich, F. Seitz, and D. Turnbull (Academic, London, 1974), pp. 235-319.
[17]S. Asano and F. Yonezawa, J. Phys. F **10**, 75 (1980).
[18]S. F. Edwards, Proc. Phys. Soc. **86**, 977 (1965).
[19]P. Lloyd, Proc. Phys. Soc. **86**, 825 (1965).
[20]P. Lloyd, Proc. Phys. Soc. **90**, 207 (1967).
[21]J. Rubio, J. Phys. C **2**, 288 (1969).
[22]N. W. Ashcroft and W. Schaich, Phys. Rev. B **1**, 1370 (1970).
[23]L. Schwartz and H. Ehrenreich, Ann. Phys. (N.Y.) **64**, 100 (1971).
[24]N. Szabo, J. Phys. C **5**, L241 (1972).
[25]S. F. Edwards, in *The Properties of Liquid Metals,* edited by S. Takeuchi (Wiley, New York, 1973).
[26]R. Evans, B. L. Gyorffy, N. Szabo, and J. M. Ziman, in *The Properties of Liquid Metals,* edited by S. Takeuchi (Wiley, New York, 1973).
[27]B. L. Gyorffy, in Proceedings of the Mount Tremblant International Summer School, 1973 (unpublished).
[28]J. S. Rousseau, J. C. Stoddart, and N. H. March, in *The Properties of Liquid Metals,* edited by S. Takeuchi (Wiley, New York, 1973).
[29]N. Szabo, J. Phys. C **6**, L437 (1973).
[30]D. B. Boercker, F. J. Rogers, and H. E. DeWitt, Phys. Rev. A **25**, 1623 (1982).
[31]G. A. Rinker, Los Alamos National Laboratory Report LA-9872-MS, January, 1984 (unpublished).
[32]See AIP document no. PAPS PRBMD-31-4207-33 for 33 pages of technical appendices. Order by PAPS number and journal reference from American Institute of Physics, Physics Physics Auxiliary Publication Service, 335 East 45th Street, New York, N.Y. 10017. The price is $1.50 for a microfiche, or $5.00 for a photocopy. Airmail additional. Make checks payable to the American Institute of Physics.
[33]P. W. Anderson and W. L. McMillan, in *Proceedings of the International School of Physics, Enrico Fermi, Course XXXVII,* edited by W. Marshall (Academic, London, 1967).
[34]E. De Dycker and P. Phariseau, in *The Properties of Liquid*

Metals, edited by S. Takeuchi (Wiley, New York, 1973).
[35]P. L. Taylor and G. Bambakidis, in *The Properties of Liquid Metals,* edited by S. Takeuchi (Wiley, New York, 1973).
[36]J. J. Olson, Phys. Rev. B **12**, 2908 (1975).
[37]E. Esposito, H. Ehrenreich, and C. D. Gelatt, Jr., Phys. Rev. B **18**, 3913 (1978).
[38]J. S. Brown, J. Phys. F **11**, 2099 (1981).
[39]M. Itoh and M. Watabe, J. Phys. F. **14**, L9 (1984).
[40]G. E. Brown and D. G. Ravenhall, Proc. R. Soc. London, Ser. A **208**, 552 (1951).
[41]A. O. E. Animalu and V. Heine, Philos. Mag. **12**, 1249 (1965).
[42]L. J. Sundström, Philos. Mag. **11**, 657 (1965).
[43]D. M. North and C. N. J. Wagner, Phys. Lett. **30A**, 440 (1969).
[44]J. B. Van Zytveld, J. E. Enderby, and E. W. Collings, J. Phys. F **2**, 73 (1972).
[45]A. O. E. Animalu, in *The Properties of Liquid Metals,* edited by S. Takeuchi (Wiley, New York, 1973).
[46]M. Appapillai and A. R. Williams, J. Phys. F **3**, 759 (1973).
[47]W. A. Harrison, in *The Properties of Liquid Metals,* edited by S. Takeuchi (Wiley, New York, 1973).
[48]A. Meyer, C. W. Nestor, Jr., and W. H. Young, in *The Properties of Liquid Metals,* edited by S. Takeuchi (Wiley, New York, 1973).
[49]A. R. Williams and M. Appapillai, J. Phys. F **3**, 772 (1973).
[50]N. W. Ashcroft and D. Stroud, in *Theory of the Thermodynamics of Simple Liquid Metals,* Vol. 33 of *Solid State Physics: Advances in Research and Applications,* edited by H. Ehrenreich, F. Seitz, and D. Turnbull (Academic, New York, 1978), pp. 1—81.
[51]J. A. Moriarty, Phys. Rev. B **1**, 1363 (1970).
[52]J. A. Moriarty, Phys. Rev. B **26**, 1754 (1982).
[53]J. E. Enderby and N. H. March, in *The Properties of Liquid Metals,* edited by S. Takeuchi (Wiley, New York, 1973).
[54]D. A. Liberman, D. T. Cromer, and J. T. Waber, Comput. Phys. Commun. **2**, 107 (1971).
[55]R. D. Cowan and J. Ashkin, Phys. Rev. **105**, 144 (1957).
[56]D. A. Liberman, Phys. Rev. B **20**, 4981 (1979); J. Quant. Spectrosc. Rad. Transfer **27**, 335 (1982).
[57]R. Latter, Phys. Rev. **99**, 510 (1955).
[58]D. A. Liberman, Phys. Rev. B **2**, 244 (1970).
[59]W. Kohn and L. J. Sham, Phys. Rev. **140**, A1133 (1965).
[60]L. J. Sham and W. Kohn, Phys. Rev. **145**, 561 (1966).
[61]D. A. Liberman, Phys. Rev. **171**, 1 (1968).
[62]N. S. Gingrich and L. Heaton, J. Chem. Phys. **34**, 873 (1961).
[63]M. S. Wertheim, Phys. Rev. Lett. **10**, 321 (1963).
[64]M. S. Wertheim, J. Math. Phys. **5**, 643 (1964).
[65]W. R. Smith and D. Henderson, Mol. Phys. **19**, 411 (1970).
[66]D. Henderson and E. W. Grundke, J. Chem. Phys. **63**, 601 (1975).
[67]R. G. Palmer and J. D. Weeks, J. Chem. Phys. **58**, 4171 (1973).
[68]M. Parrinello and M. P. Tosi, Riv. Nuovo Cimento **2**, No. 6, 1 (1979).
[69]F. J. Rogers, D. A. Young, H. E. DeWitt, and M. Ross, Phys. Rev. A **28**, 2990 (1983).
[70]Y. Rosenfeld and N. W. Ashcroft, Phys. Rev. A **20**, 1208 (1979).
[71]J. Friedel, J. Phys. F **3**, 785 (1973).
[72]J. Keller and R. Jones, J. Phys. F **1**, L33 (1971).
[73]F. Cyrot-Lackmann, in *The Properties of Liquid Metals,* edited by S. Takeuchi (Wiley, New York, 1973).
[74]N. H. Fletcher, in *The Properties of Liquid Metals,* edited by S. Takeuchi (Wiley, New York, 1973).
[75]D. House and P. V. Smith, J. Phys. F **3**, 753 (1973).
[76]W. B. Hubbard, Astrophys. J. **146**, 858 (1966).
[77]M. Lampe, Phys. Rev. **170**, 306 (1968).
[78]M. Lampe, Phys. Rev. **174**, 276 (1968).
[79]W. B. Hubbard and M. Lampe, Astrophys. J. Suppl. Ser. **18**, 297 (1969).
[80]E. A. Uehling and G. E. Uhlenbeck, Phys. Rev. **43**, 552 (1933).
[81]E. A. Uehling, Phys. Rev. **46**, 917 (1934).
[82]R. Landshoff, Phys. Rev. **76**, 904 (1949).
[83]R. S. Cohen, L. Spitzer, Jr., and P. McR. Routly, Phys. Rev. **80**, 230 (1950).
[84]L. Spitzer and R. Härm, Phys. Rev. **89**, 977 (1953).
[85]S. I. Braginskii, Rev. Plasma Phys. 1 205 (1965).
[86]E. Flowers and N. Itoh, Astrophys. J. **206**, 218 (1976).
[87]E. Flowers and N. Itoh, Astrophys. J. **230**, 847 (1979).
[88]E. Flowers and N. Itoh, Astrophys. J. **250**, 750 (1981).
[89]F. J. Rogers, H. E. DeWitt, and D. B. Boercker, Phys. Lett. **82A**, 331 (1981).
[90]R. M. More, in *Applied Atomic Collision Physics II* (Academic, London, 1982).
[91]R. M. More, in Proceedings of the NATO Workshop Conference on Atomic and Molecular Processes in Controlled Fusion, Palermo, Sicily, 1982 (in press).
[92]Y. T. Lee and R. M. More, Phys. Fluids **27**, 1273 (1983).
[93]H. M. Van Horn, Astrophys. J. **151**, 227 (1968).
[94]D. G. Yakovlev and V. A. Urpin, Astron. Zh. **52**, 526 (1980) [Sov. Astron. **24**, 303 (1980)].